Selenium Nanoparticles as a Carrier of 5-Fluorouracil to Achieve Anticancer Synergism

Wen Liu,[†,#] Xiaoling Li,[†,#] Yum-Shing Wong,[‡] Wenjie Zheng,[†,*] Yibo Zhang,[†] Wenqiang Cao,[†] and Tianfeng Chen[†,*]

[†]Department of Chemistry, Jinan University, Guangzhou 510632, China and [‡]School of Life Sciences, The Chinese University of Hong Kong, Hong Kong, China. [#]These authors contributed equally to the work.

ABSTRACT

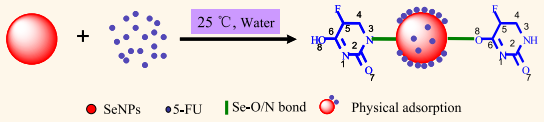

A simple method for preparing 5-fluorouracil surface-functionalized selenium nanoparticles (5FU-SeNPs) with enhanced anticancer activity has been demonstrated in the present study. Spherical SeNPs were capped with 5FU through formation of Se—O and Se—N bonds and physical adsorption, leading to the stable structure of the conjugates. 5FU surface decoration significantly enhanced the cellular uptake of SeNPs through endocytosis. A panel of five human cancer cell lines was shown to be susceptible to 5FU-SeNPs, with IC_{50} values ranging from 6.2 to 14.4 μM. Despite this potency, 5FU-SeNP possesses great selectivity between cancer and normal cells. Induction of apoptosis in A375 human melanoma cells by 5FU-SeNPs was evidenced by accumulation of sub-G1 cell population, DNA fragmentation, and nuclear condensation. The contribution of the intrinsic apoptotic pathway to the cell apoptosis was confirmed by activation of caspase-9 and depletion of mitochondrial membrane potential. Pretreatment of cells with a general caspase inhibitor z-VAD-fmk significantly prevented 5FU-SeNP-induced apoptosis, indicating that 5FU-SeNP induced caspase-dependent apoptosis in A375 cells. Furthermore, 5FU-SeNP-induced apoptosis was found dependent on ROS generation. Our results suggest that the strategy to use SeNPs as a carrier of 5FU could be a highly efficient way to achieve anticancer synergism. 5FU-SeNPs may be a candidate for further evaluation as a chemopreventive and chemotherapeutic agent for human cancers, especially melanoma.

KEYWORDS: selenium nanoparticles · 5-fluorouracil · cellular uptake · synergistic effects · apoptosis

Cancer is a growing health problem around the world, particularly with the steady rise in life expectancy, increasing urbanization, and the subsequent changes in environmental conditions and lifestyle.[1] Fortunately, diagnostic equipments and therapeutic technology have been improved and the mortality has decreased in the past few years.[2] But the current cancer treatments often kill healthy cells and thus show significant toxicity and unavoidable side effects.[3] The emergence of bionanomaterials gave a new prospect to the researchers who have always been looking for methods to solve these problems. The combination of biotechnology and nanotechnology has led to the development of an interdisciplinary area, bionanotechnology, which shows broad applications in molecular imaging, molecular diagnosis, and targeted therapy. The basic rationale is that nanoscaled materials have optical, magnetic, or structural properties that are not available from molecules or bulk solids. The excellent performance of bionanomaterials opens novel horizons for drug delivery and therapy of diseases that have traditionally been recognized as incurable *via* basic therapies or surgical methods, especially for cancers.[4]

Selenium (Se) is an essential trace element with important physiological functions and extensive pharmacological actions. Many studies have shown that the supplementation of Se could prevent cancer and reduce cancer incidence.[5−7] Although clinical trials with Se are currently limited to cancer chemoprevention, recent evidence strongly showed the potential for utilization of Se in a new way, to overt cancer through a combination with well-established chemotherapeutic and hormonal agents.[8,9] Many studies showed that Se could sensitize cancer cells to conventionally used anticancer drugs. For instance, Hu and co-workers reported that Se compounds could enhance the efficacy of paclitaxel against hormone refractory prostate cancer *in vitro* and *in vivo*. At the same time, Se compounds may be a novel agent to improve taxane combination therapy.[8] Song Li *et al*. reported that overexpression of Akt blocked the ability of Se/doxorubicin to induce breast cancer cell apoptosis.[9] These results demonstrated that selenocompounds were a highly effective

* Address correspondence to tchentf@jnu.edu.cn, tzhwj@jnu.edu.cn.

Received for review July 2, 2011 and accepted July 23, 2012.

Published online July 23, 2012
10.1021/nn202452c

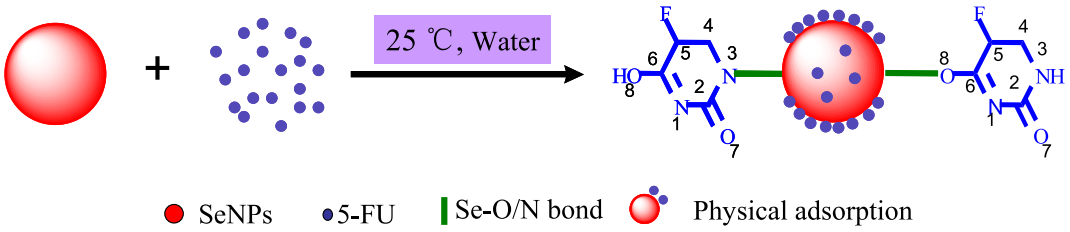

Scheme 1. Schematic illustration for preparation of 5FU-SeNPs.

modulator of the therapeutic efficacy and selectivity of anticancer drugs. However, Se displayed a narrow margin between the beneficial and toxic effects. As an anticancer agent, the effective dose of Se is close to the toxic range, which greatly limits its clinical application. Although regarded as an essential trace element, Se is toxic if taken in excess. Studies have showed that exceeding the tolerable upper intake level of 400 μg per day can lead to selenosis.[5−7] For instance, symptoms of selenosis in susceptible patients have been found at or above 819 ± 126 μg Se/day.[10] In contrast, a human trial performed by Reid *et al.* showed no obvious selenosis in patients who received 1600 μg Se/day in selenized yeast, in which selenomethionine (SeM) was the major Se species. Only some symptoms of Se toxicity in patients who received 3200 μg Se/day did occur.[11] Studies also showed that bovine albumin protein-coated Se nanoparticles (BSA-SeNPs) exhibited comparable efficacy to SeM and Se-methylselenocysteine (SeMSC) in upregulating selenoenzymes and tissue Se levels, but was less toxic in comparison with the organic Se compounds.[12,13] Therefore, the beneficial and toxic effects of Se on human health are strongly dependent on its concentration and chemical form.

Numerous investigations have shown that both tissue and cell distribution profiles of anticancer drugs could be improved by nanotechnology.[14] Nanolized anticancer drugs displayed increased antitumor efficiency and reduced serious side effects.[15] Zhang *et al.* reported that as compared to Se-methylselenocysteine, SeNPs showed equal efficacy in increasing the activities of antioxidant enzymes, but had much lower toxicity.[13] The *in vitro* free radical scavenging efficiency of SeNPs was also found higher than organic and inorganic selenocompounds.[12,16,17] For instance, based on the data of LD_{50}, the *in vivo* toxicity of SeNPs was about 4−6 times lower than SeM and SeMSC.[12,13,17] Therefore, SeNPs may have a much wider margin between beneficial and toxic effects than other selenocompounds, and could serve as a potential chemopreventive agent with reduced risk of toxicity.

5-Fluorouracil (5FU) is a widely used chemotherapy drug for treatment of lung, liver, bladder, skin, colon, pancreatic, breast and head and neck cancers.[18−22] The concentrations of 5FU in the liver, peritoneum, stomach, and intestine were high after intravenous administration, so the tumors in the digestive system could be more effectively treated by this drug.[23] However, the side effects, mainly reflected by liver damage and digestive discomfort, limit the improvement of the efficacy. Interestingly, Thant and co-workers found that Se played a very important role in the joint action with 5FU to overcome the drug resistance in colon cancer.[24] Schroeder and co-workers found that the toxicity of 5FU, oxaliplatin and irinotecan against HCT116 colon cancer cells increased significantly by 1.1, 2.7, and 2.6 times through combination with selenite.[25] Rustum *et al.* reported that Se could reduce the toxicity induced by the anticancer drugs, like taxol, cisplatin, 5FU, and anthracycline.[26] Therefore, we look forward to design a synergistic system by conjugation of 5FU to the surface of the SeNPs, in which SeNPs could enhance the cure rate of 5FU and lower its toxicity. The *in vitro* anticancer activity and the underlying mechanisms of 5FU-SeNPs against human cancer cells were also examined. Our results showed that 5FU surface decoration significantly enhanced the cellular uptake of SeNPs through endocytosis. 5FU-SeNPs effectively inhibited the cancer cell growth and possessed great selectivity between cancer and normal cells. Further investigation on intracellular mechanisms found that 5FU-SeNPs triggered caspase-dependent and ROS-dependent apoptosis in A375 cells through mitochondria-mediated pathways.

RESULTS AND DISCUSSION

Morphology and Stability of 5FU-SeNPs. In the present study, we demonstrated a simple method to synthesize 5FU-functionalized SeNPs through conjugation of 5FU to the surface of the nanoparticles. SeNPs were capped with 5FU molecules to form more compact and stable globular nanocomposites (Scheme 1). The morphology and chemical composition of 5FU-SeNPs were characterized using various spectroscopic and microscopic methods. Figure 1 shows the TEM images of the SeNPs with the absence (A, B) and presence (C, D) of the capping agents 5FU, which clearly revealed that 5FU-SeNPs presented monodisperse and homogeneous spherical structure with an average diameter of about 70 nm, whereas SeNPs in aqueous solutions were badly aggregated due to their high surface energy, thus resulting in significant precipitation. These results suggest that the presence of 5FU is a

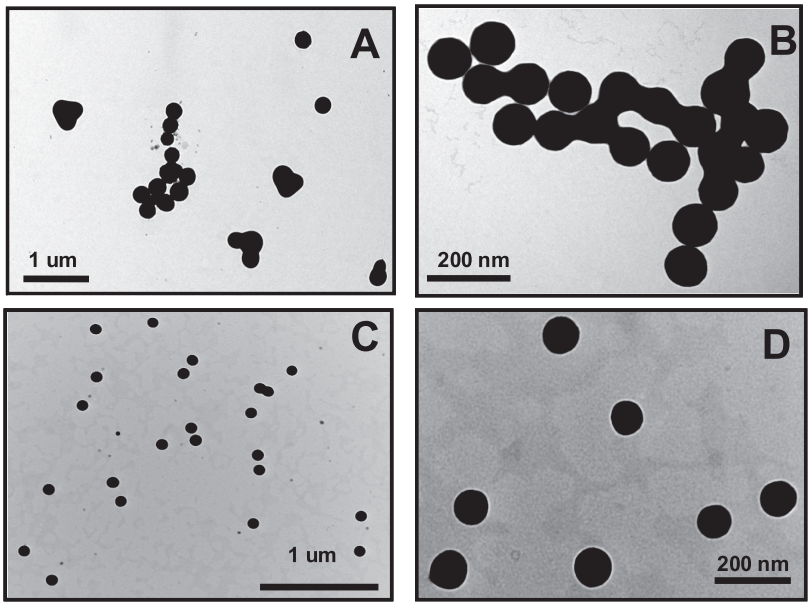

Figure 1. TEM images of SeNPs (A and B) and 5FU-SeNPs (C and D).

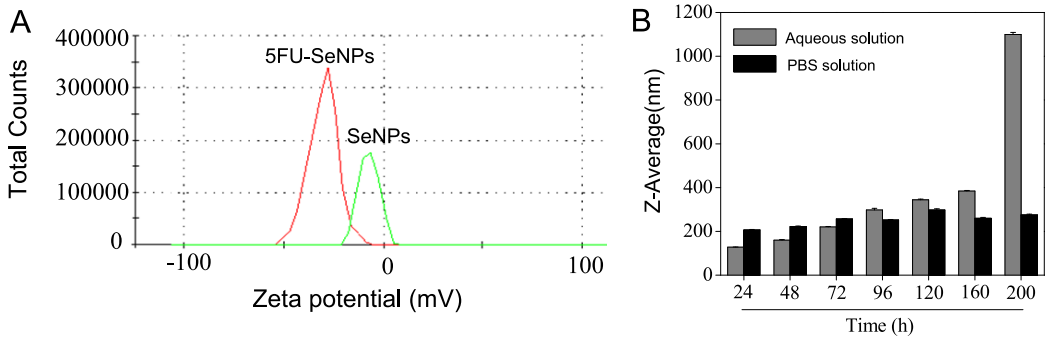

Figure 2. Zeta potential of SeNPs and 5FU-SeNPs (A) and stability of 5FU-SeNPs in aqueous and PBS (pH = 7.4) solutions (B).

key factor in regulating and controlling the size of the SeNPs.

Stability is an important issue for the nanoparticles future applications.[27,28] To examine the effects of 5FU on the surface properties and stability of SeNPs, we measured the zeta potential and size distribution of SeNPs and 5FU-SeNPs. As shown in Figure 2A, the zeta potential of SeNPs was −7.1 mV, which decreased to −30.0 mV after the 5FU surface decoration, explaining the higher stability of 5FU-SeNPs than SeNPs. Furthermore, we used Zetasizer Nano-ZS particle analyzer to test the changes in size distribution of 5FU-SeNPs in both aqueous and physiological conditions. The results revealed that, 5FU-SeNPs remained stable until the time of 160 h in aqueous solutions. However, when the reaction time increased to 200 h, the sizes of 5FU-SeNPs increased dramatically, and the aggregation of the nanoparticles began to happen (Figure 2B). In contrast, under the physiological conditions (PBS, pH = 7.4), 5FU-SeNPs remained stable at least for 200 h. The hydrodynamic diameter was distributed between 200 and 280 nm, and no aggregation and precipitation were observed. The high stability of 5FU-SeNPs under physiological condition supports their future medical applications.[29]

Chemical Composition and Sturcture of 5FU-SeNP. An elemental composition analysis employing EDX showed the presence of a strong signal from the Se atoms (57.1%), together with F atom signal (2.3%), C (23.6%), N (8.1%), and O (8.9%) that from 5FU molecules. No obvious peaks for other elements or impurities were observed. The presence of an F atom indicate that 5FU as been conjugated to the surface of SeNPs (Figure 3A). On the basis of the results of EDX analysis, the representative chemical formula of 5FU-SeNPs is derived as $(Se_6 5FU)_n$. 5FU-SeNP was further characterized by FTIR to confirm the formation of chemical bonds between 5FU and Se that occurred during the synthesis reaction.[30] As shown in Figure 3B, the FT-IR spectrum of 5FU-SeNPs resembles those of 5FU and SeNPs, giving clear evidence that 5FU and SeNPs form parts of the nanocomposite. In the spectrum of 5FU, the peaks at 1723 and 1672 cm^{-1} were assigned to the stretching vibration of C═O, while the peak at

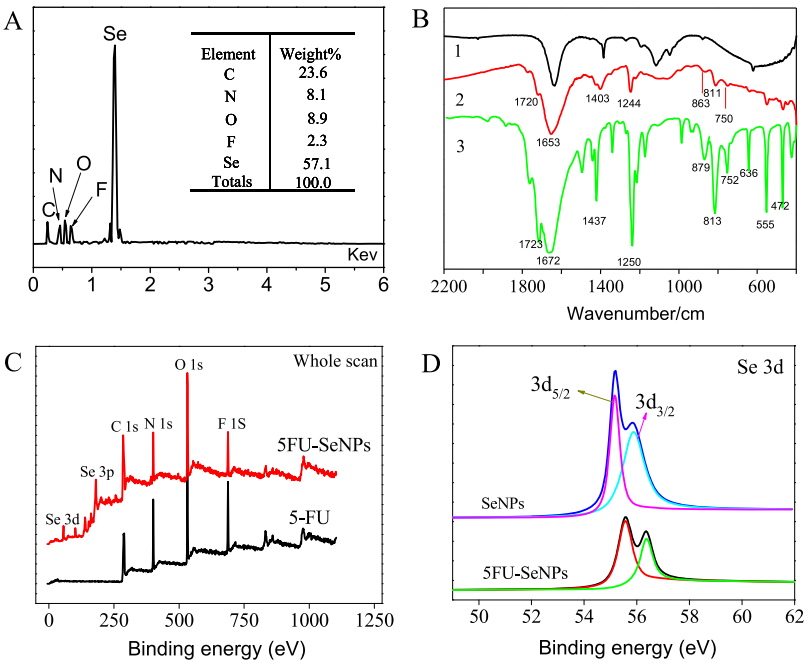

Figure 3. Chemical composition and structure characterization of 5FU-SeNPs: (A) EDX analysis of 5FU-SeNPs; (B) FT-IR spectra of SeNPs (1), 5FU-SeNPs (2), and 5FU (3); (C) XPS spectra of 5FU and 5FU-SeNPs; (D) Se 3d spectra of SeNPs and 5FU-SeNPs.

1245 cm^{-1} corresponded to the stretching vibration of C—N. The peaks at 1437 cm^{-1} were assigned to the stretching vibration of —C—F.[31] The appearance of the above peaks, with the addition of the peaks at 879, 813, 555, and 472 cm^{-1} in the spectrum of 5FU-SeNPs confirmed the presence of 5FU on the surface of SeNPs.[32,33] Moreover, blue shift was observed for the groups of C═O and C—N in 5FU-SeNPs, which could be due to the formation of Se—O and Se—N bonds.

The XPS spectra were also recorded to examine the interaction between 5FU and SeNPs. As shown in Figure 3C, the presence of F 1s peak at 688.02 eV in the spectrum of 5FU-SeNPs further confirmed that 5FU has been successfully conjugated to the SeNP. The peaks of Se $3d_{5/2}$ and $3d_{3/2}$ also increased from 55.17 and 55.99 eV (SeNPs) to 55.48 and 56.29 eV (5FU-SeNPs), respectively (Figure 3D), indicating that the Se 3d orbit participates in bonding in formation of 5FU-SeNPs. Moreover, the increase in the energy of O 1s and N 1s was also observed in the spectrum of 5FU-SeNPs (Figure 3C). Interestingly, in the fitting spectrum of O 1s (Supporting Information, Figure S1), the peak in 5FU-SeNPs split into two. One peak at 532.2 eV possibly come from the molecule of 5FU, and its shift to 531.4 eV may correspond to the formation of a Se—O band. Taken together, the changes in the XPS and FT-IR spectra support the formation of Se—O and Se—N bonds in 5FU-SeNPs.

5FU Surface Decoration Enhances Cellular Uptake of SeNPs. An important factor that usually contributes to nanomaterial-based drug cytotoxicity is cellular uptake. Nanomaterials tend to accumulate in cancer cells through a passive targeting process and often serve as "nanocarriers" for chemotherapeutics. However, this passive strategy has limitations due to its random delivery mode.[3] Studies have showed that 5FU distributed as a weak acid in aqueous solutions and its uptake by cancer cells involved facilitated transport *via* the uracil transporter.[34] Yamamoto and Kawasaki found that the uptake of 5FU was directly coupled to the ATP derived from glycolysis.[35,36] Therefore, a quantitative analysis of cellular uptake was conducted in this study by measuring the fluorescence intensity from intracellular coumarin-6 loaded nanoparticles. Human melanoma A375 cells were used as a model to investigate the internalization of 6-coumarin loaded 5FU-SeNPs. The cells were incubated with different concentrations of nanoparticles and examined by fluorescence microscopy and real-time living cell imaging. As shown in Figure 4A, the green fluorescence from the nanoparticles penetrated into the A375 cells in a dose-dependent manner after incubation with the nanoparticles for 2 h. Most of the nanoparticles were internalized into the cytoplasm of the cells. Experiments were conducted to examine the internalization of 5FU-SeNPs in A375 cells by real-time living cell microscopy. The images obtained from the FITC channel show the green fluorescence of the coumarin-6 loaded nanoparticles. Cellular uptake of the nanoparticles displayed a rapid onset after 10-min of treatment, followed by a progressive increase to 2 h. 5FU-SeNPs with green fluorescence entered the cells after 10 min of treatment and penetrated into the cytoplasm at 20 min. The intracellular nanoparticles increased after that in a time-dependent manner (Figure 4B). Using DAPI as a marker of nucleus, we showed that, the cell nuclei

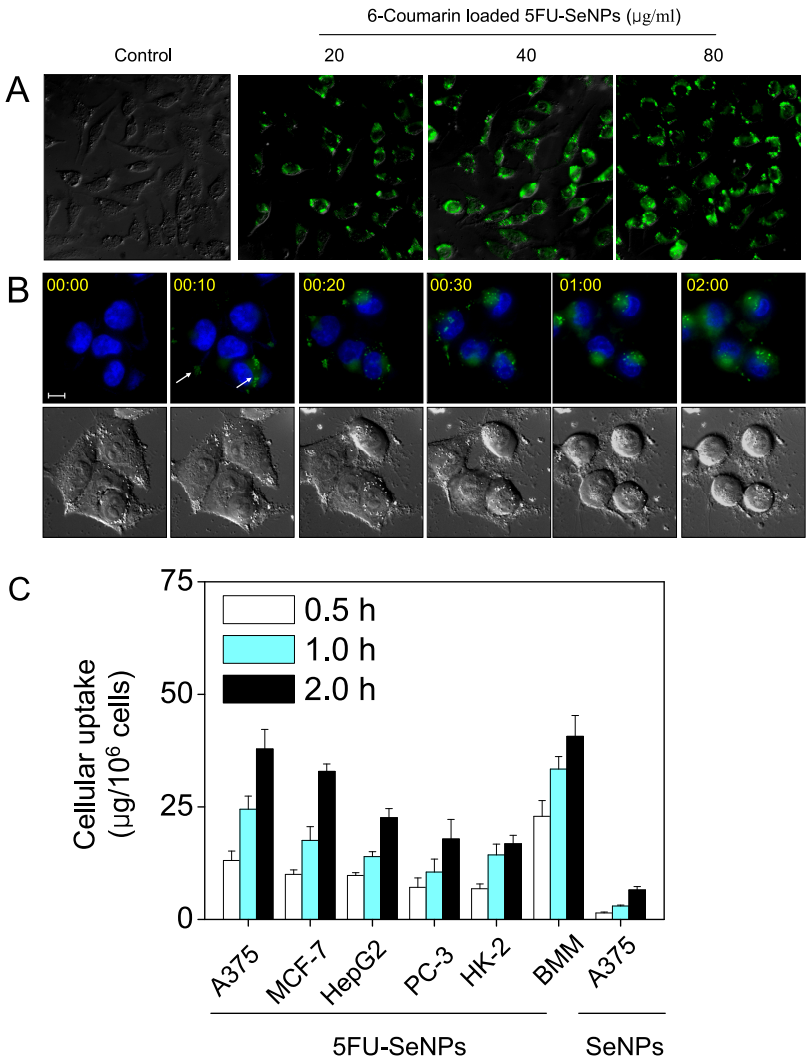

Figure 4. (A) Fluorescence microscope images show the internalization of 6-coumarin loaded nanoparticles (green fluorescence) in A375 cells after 2 h incubation. (B) Real-time imaging of the same A375 cells treated with 40 μg/mL 6-coumarin loaded nanoparticles. The cell morphology was captured by a differential internal reflection (DIC) microscope. The nanoparticles and cell nucleus were visualized by green and blue fluorescence, respectively. The upper panel is the merged images of nanoparticles and the nucleus and the lower panels are DIC images. Scale bar: 10 μm. (C) Quantitative analysis of cellular uptake efficiency of 6-coumarin loaded 5FU-SeNPs and SeNPs at 80 μg/mL in various cancer and normal cells after 2-h incubation. Values expressed are means $\pm$ standard deviation of triplicates.

were circumvented by green fluorescence, and we did not observe the overlay of green and blue fluorescence (Figure 4B), suggesting that the nuclei were not the cellular target of 5FU-SeNPs.

It should be pointed out that no fluorescence could be detected under the FITC channel in the cells exposed to the SeNPs under the conditions used in the experiments, which enabled us to determine the intracellular 5FU-SeNP concentrations based on the fluorescence intensity of coumarin-6 in different cancer and normal cell lines. Briefly, the cells seeded in 96-well plates were incubated with 80 μg/mL of coumarin-6 loaded 5FU-SeNPs for 0.5, 1.0, and 2.0 h, and the concentrations of nanoparticles were determined by using a fluorescence microplate reader with excitation and emission wavelengths set at 430 and 485 nm, respectively. As shown in Figure 4C, intracellular 5FU-SeNP concentrations increased in a time-dependent manner in all of the tested cell lines. For instance, after 0.5, 1.0, and 2.0 h incubation with 80 μg/mL 6-coumarin loaded nanoparticles, the concentrations of 5FU-SeNPs in A375 cells increased to 13.1, 24.5, and 37.9 μg/10^6 cells, respectively, which were about 6−9 times of those of SeNPs without 5FU surface decoration. These results indicate that 5FU surface decoration enhances the cellular uptake of SeNPs. Moreover, we used primary culture BMM cells as a macrophage model to examine the cellular uptake of 5FU-SeNPs in normal cells. As we expected, the cellular uptake of 5FU-SeNPs by BMM was higher than those of other cell lines, including A375, MCF-7, HepG2, and HK-2 cells. Interestingly, we also found that addition of excess free 5-FU inhibited the cellular uptake of 5FU-SeNPs in A375 cells in a dose-dependent manner

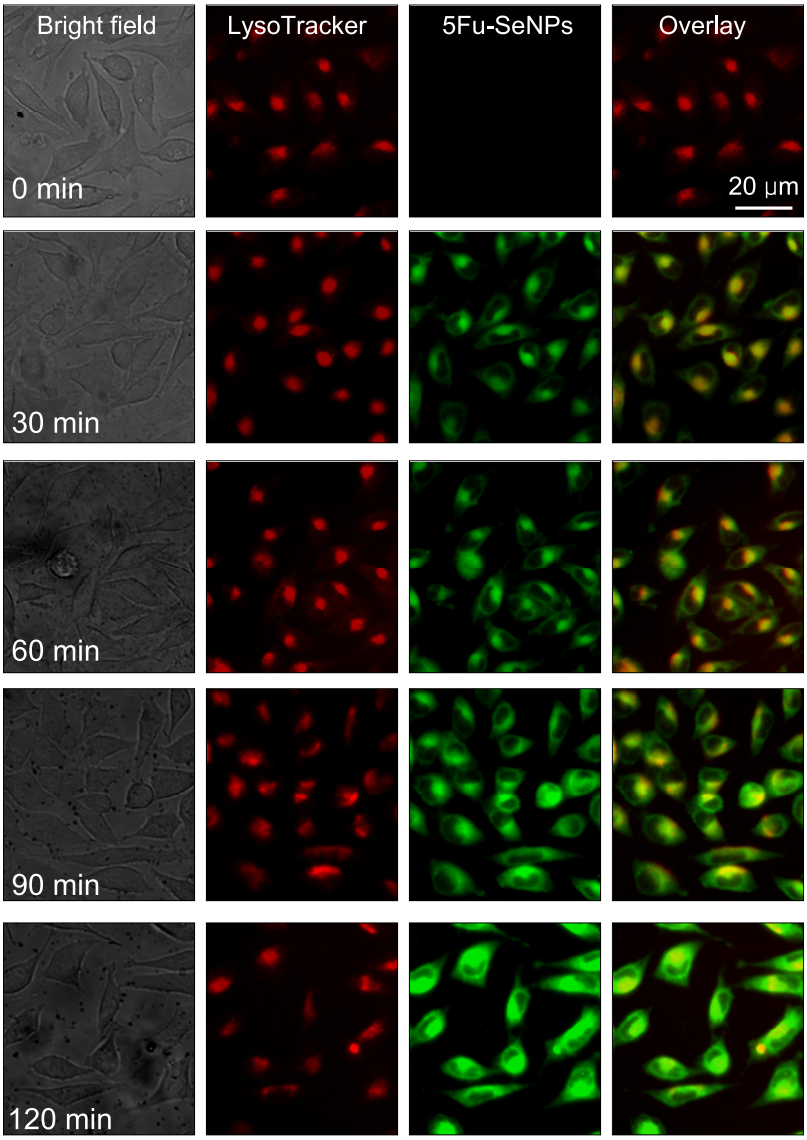

Figure 5. Colocalization of 5FU-SeNPs (green fluorescence) and lysosomes (red fluorescence) in A375 cells. The cells were treated with 40 μg/mL 6-coumarin loaded nanoparticles for different periods of time and visualized under a fluorescence microscope.

(Supporting Information, Figure S3), which demonstrates the important role of 5FU in the internalization process of 5FU-SeNPs.

Localization and Uptake Pathways of 5FU-SeNPs. Endocytosis is one of the important entry mechanisms for extracellular materials, particularly nanomaterials.[37] In this study, the localization of 5FU-SeNPs in cancer cells was investigated by using a specific probe, Lyso Tracker Red, for fluorescence imaging of the lysosomes. As shown in Figure 5, the combination of the green and red fluorescence clearly indicates the colocalization of 5FU-SeNPs and lysosomes in A375 cells. These results suggest that lysosomes are the main target organelles of 5FU-SeNPs. 5FU-SeNPs located in the lysosomes increased in a time-dependent manner. Moreover, it is noteworthy that some 5FU-SeNPs were capable of escaping from the lysosomes and were released into the cytoplasm.

The uptake pathways of nanomaterials have important impact on their bioactivities. Therefore, specific endocytosis inhibitors were used to examine the internalization mechanisms and uptake pathways of 5FU-SeNPs in A375 cells. As shown in Figure 6, treatments with sodium azide (NaN_3) and 2-deoxy-D-glucose (DOG), or at low temperature of 4 °C instead of 37 °C, markedly reduced the cellular uptake of 5FU-SeNPs to 29.9% and 26.5% of the control, demonstrating that 5FU-SeNPs entered A375 cells *via* energy-dependent endocytosis. In living cells, the endocytosis encompasses three major pathways, including macropinocytosis/phagocytosis and clathrin-mediated and caveolae-mediated endocytosis. Since A375 human melanoma cells are known not to be phagocytic, the studies that followed were focused on the other two pathways. The specific inhibitors of clathrin-mediated endocytosis,

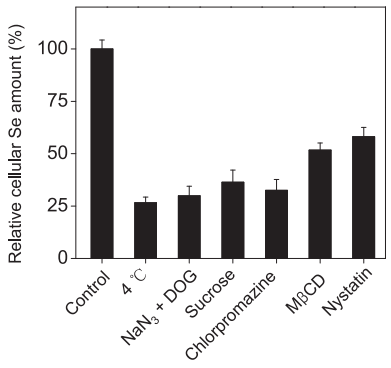

Figure 6. Cellular amount of Se in A375 cells after 4-h incubation with 5FU-SeNPs. Cells were incubated either at 37 °C (control) or at 4 °C. Prior to the incubation with 5FU-SeNPs, cells were pretreated with specific endocytosis inhibitors for different periods of time.

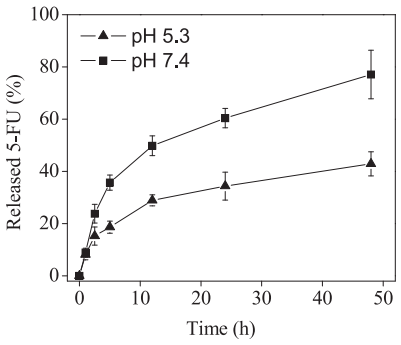

Figure 7. *In vitro* release profiles of 5-FU from 5FU-SeNPs in DMEM cell culture medium with 10% serum. The 5Fu concentrations were determined by HPLC analysis.

sucrose and chlorpromazine, strongly decreased the endocytosis of 5FU-SeNPs in A375 cells to 36.4% and 32.5% of the control, suggesting that the main pathway is clathrin-mediated endocytosis. Moreover, methyl-β-cyclodextrin (MβCD) and nystatin inhibited the endocytosis of 5FU-SeNPs to 51.7% and 58.1% of the control, showing that caveolae-mediated endocytosis also plays an important role in internalization of 5FU-SeNPs. Therefore, both clathrin- and caveolae-mediated pathways are involved in the cellular uptake of 5FU-SeNPs in A375 cells.

pH-Mediated Drug Release of 5FU *in vitro*. The *in vitro* drug release of 5FU from 5FU-SeNPs in DMEM cell culture medium with 10% serum at pH of 7.4 and 5.3 was investigated to simulate the normal body blood and acidic environments. Figure 7 showed the release profiles of 5FU from the nanoparticles into the culture medium. The cumulative release of 5FU mainly occurred in the first 12 h under two pH systems, which reached 48.9% at pH 5.3 and 28.9% at pH 7.4 within 12 h, respectively. Thereafter, the cumulative release of 5FU reached 77.1% at pH 5.3 and 42.9% at pH 7.4 for 48 h, respectively. This initial burst of 5FU release could be partly attributed to the weak bonds or the adsorption of drugs on the surface of nanoparticles.[38] The results also demonstrated that the release process at pH 7.4 was much slower than that at pH 5.3. One of possible reasons was the low solubility of 5FU at pH 7.4 than that at pH 5.3. Moreover, in the PBS system without serum, 5FU was released into the PBS solution in a time-dependent manner in the initial 60 min (Supporting Information, Figure S4). After 60-min incubation, about 50% of 5FU has been released from the nanoparticles. A slow increase in drug release was then observed from 60 to 300 min. At the time point of 300 min, 70.9% of 5FU has been released into the solution from 5FU-SeNPs. The release of 5FU was much faster in the dynamic condition than that in the static condition.

In a comparison of the release of 5FU in culture medium and PBS solution, the decrease in 5FU release in cell culture medium with the presence of serum could be partly attributed to adsorption of proteins, such as BSA, to the surface of the nanoparticles, which formed a macromolecule shell and effectively slow down the release of 5FU into the aqueous phase. This hypothesis could be supported by the increase of the hydrodynamic diameter of 5FU-SeNPs from 207 to 262 nm after the addition of serum into the PBS solutions (data not shown). Interestingly, a faster release of 5FU has been observed under acidic conditions (pH = 5.3), which is exactly what we expect. 5FU could principally be distributed around tumor tissues with an acidic microenvironment rather than in the normal section. Taken together, these results demonstrate that SeNPs hold a promise as a pH-mediated release delivery vehicle for potential cancer therapy.

Induction of Apoptotic Cell Death by 5FU-SeNPs. The *in vitro* cytotoxic effects of 5FU-SeNPs were first screened against various human cancer cell lines by MTT assay. As shown in Figure 8A, 5FU-SeNPs exhibited a broad-spectrum inhibition against A375, MCF-7, HepG2, Colo201, and PC-3 cancer cells with IC_{50} values ranging from 6.2 to 14.4 μM. Despite this potency, 5FU-SeNPs showed lower cytotoxicity toward human normal cells (Hs68 human fibroblasts, HK-2 proximal tubular cells, and MCF-10A human mammary epithelial cells) and bone marrow-derived macrophages (BMM), with IC_{50} values at 67.1, 88.4, 72.7, and 61.3 μM, respectively. Interestingly, MCF-10A cells were used as a model to examine the effects of 5FU-SeNPs on normal breast cells as compared to human breast cancer cells. The results showed that 5FU-SeNPs exhibited lower cytotoxicity toward MCF-10A (IC = 72.7 μM) than MCF-7 cells (IC = 6.8 μM). BMM cells were also used as a model to examine the cellular uptake and related cytotoxicity of 5FU-SeNPs in macrophages. The results showed, although higher cellular uptake has been achieved, 5FU-SeNPs exhibited much lower cytotoxicity against BMM cells. These results suggest that, the effects of 5FU-SeNPs on the human cells are cell-type specific. This selectivity could be partly due to the different protein and gene expression profiles of different cells,

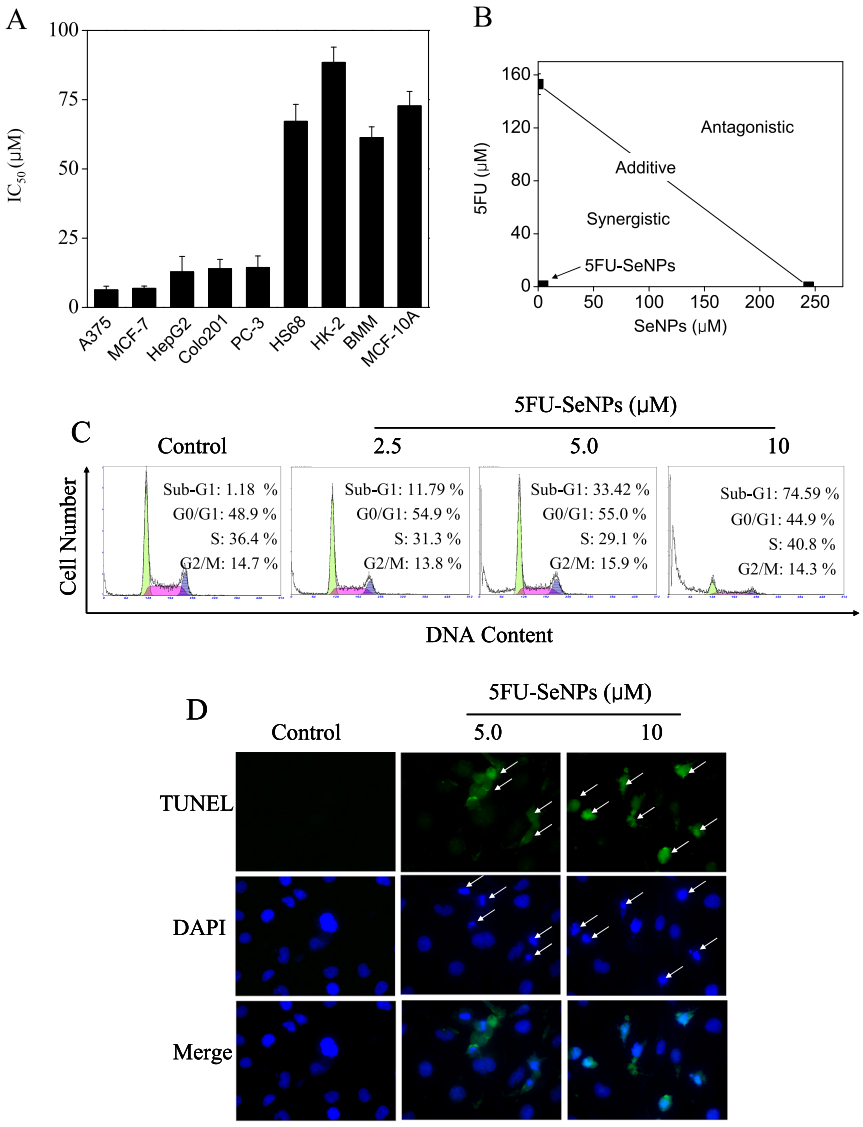

Figure 8. Induction of apoptotic cell death by 5FU-SeNPs. (A) Growth inhibition of 5FU-SeNPs on selected cancer and normal cells (72 h). Cell viability was determined by a colorimetric MTT assay. (B) Isobologram analysis of the antiproliferative effects of 5FU and SeNPs on A375 cells. (C) Fow cytometric analysis of A375 cells exposed to 5FU-SeNPs for 72 h. (D) Representative photomicrographs of DNA fragmentation and nuclear condensation (indicated by the arrows) induced by 5FU-SeNPs (24 h) as detected by TUNEL-DAPI costaining assay. The data shown here are representative of three independent experiments with similar results.

which resulted in activation of different intracellular signaling pathways after exposure to 5FU-SeNPs. Taken together, our results suggested that 5FU-SeNPs possess great selectivity between cancer and normal cells and displays potential application in cancer chemoprevention and chemotherapy.

Moreover, an *in vivo* mice model was also used to determine the acute lethal dose and acute liver injury at nonlethal dose of 5FU-SeNPs as compared to SeM. As shown in Supporting Information, Table S1, the LD50 of SeM and 5FU-SeNPs were 25.5 mg Se/kg (with 95% confidence limits of 23.1−28.1) and 108.6 mg Se/kg (with 95% confidence limits of 86.9−135.7), respectively. These results suggest that the acute toxicity of 5FU-SeNPs is much lower than that of SeM, and is comparable with that of BSA-SeNPs.[12,13] Furthermore, 5FU-SeNPs acute liver injury induced much lower acute liver injury at a nonlethal dose than SeM, which triggered a sharp elevation of ALT and AST activities in the blood of treated mice (Supporting Information, Figure S6). These results confirmed the low toxicity of 5FU-SeNPs.

The cytotoxicity of 5FU-SeNPs, 5FU, and SeNPs against the most susceptible A375 cells was investigated to examine the synergistic interaction between 5FU and SeNPs as analyzed by the isobologram method.[39] The IC_{50} values for 5FU-SeNPs, 5FU, and SeNPs were found at 6.2, 153.0, and 243.9 μM, respectively (Figure 8B). The results of the isobologram analysis revealed that the growth inhibitory effects

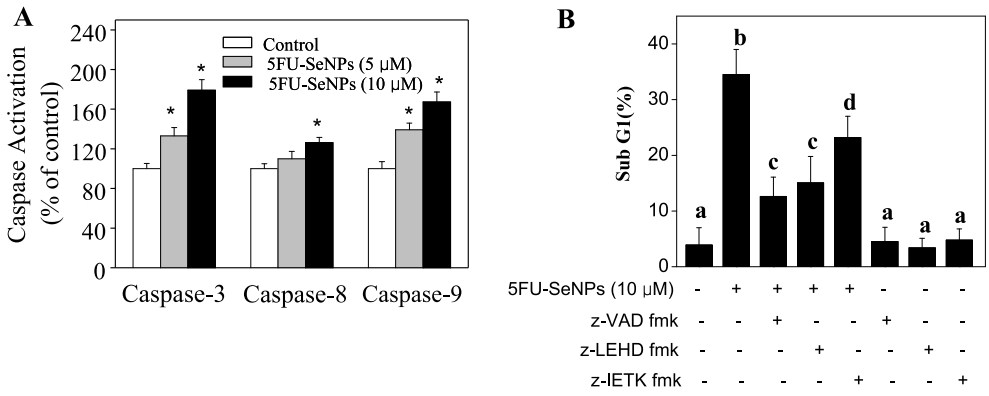

Figure 9. The 5FU-SeNP induces caspase-dependent apoptosis in A375 cells. (A) 5FU-SeNPs induced caspase activation. Cells were treated with 5FU-SeNPs for 24 h. Significant difference between treatment and control groups is indicated at $P < 0.05$ (*) level. (B) Effects of caspase inhibitors (40 μM) on apoptosis induced by 5FU-SeNPs. Cells were pretreated with z-VAD-fmk (general caspase inhibitor), z-IETD-fmk (caspase-8 inhibitor), and z-LEHD-fmk (caspase-9 inhibitor) for 2 h followed by coincubation with 5FU-SeNPs for 24 h. Apoptotic cells were determined by flow cytometry. Bars with different characters (a, b, c, and d) are statistically different at the $P < 0.05$ level.

between 5FU and SeNPs in the 5FU-SeNP system was strongly synergistic, as evidenced by the location of the data point in the isobologram being far below the line defining an additive effect. Moreover, the actual IC_{50} value of the 5FU-SeNPs (6.2 μM) was significantly lower than the theoretical one (244.9 μM). The combination index (CI) of the IC_{50} value of the 5FU-SeNPs was found at 0.024, which further confirmed the synergism between 5FU and the SeNPs.[39] Taken together, our results clearly demonstrate that the strategy to use a SeNP as a carrier of 5FU could be a highly efficient way to enhance its anticancer efficacy.

Apoptosis has been postulated as one of the most critical mechanism for the anticancer action of Se.[40] The significant biochemical characteristic of cell apoptosis is DNA fragmentation. Thus, we performed an *in vitro* apoptotic detection assay, PI-flow cytometric analysis, to determine whether apoptosis was involved in the cell death induced by the 5FU-SeNPs in the most susceptible A375 cells. Figure 8C showed the representative DNA histograms from PI staining cells, which revealed that exposure of A375 cells to different concentrations of 5FU-SeNPs for 24 h resulted in a marked dose-dependent increase in the proportion of apoptotic cells, as reflected by the increased sub-G1 populations. Apoptotic cell death was further confirmed by DNA fragmentation and nuclear condensation as detected by TUNEL enzymatic labeling and DAPI costaining assay. TUNEL can detect the early stage of DNA fragmentation in apoptotic cells prior to changes in morphology. Figure 8D showed that the 5FU-SeNPs caused a dose-dependent increase in DNA fragmentation and nuclear condensation in the A375 cells. Taken together these results indicated that the cell death induced by the 5FU-SeNPs is mainly caused by apoptosis.

5FU-SeNPs Induce Caspase-Dependent Apoptosis in A375 Cells. Caspases, a family of cysteine proteases, plays important roles in the initiation and execution of apoptosis.[40] To determine whether caspase activation is involved in the 5FU-SeNPs-induced cell death, the activities of initiator caspases (caspase-8 and caspase-9) and effector caspases-3 were examined by fluorometric assays. Figure 9A showed that the 5FU-SeNPs evoked activation of caspase-3, caspase-8, and caspase-9 in the A375 cells in a dose-dependent manner, which suggests that both intrinsic and extrinsic apoptotic pathways were involved in the 5FU-SeNP-induced apoptosis. The activity of caspase-9 (1.4–1.7 folds) increased significantly higher than those of caspases-8 (1.1–1.3 folds) in response to the 5FU-SeNPs treatments, indicating that the contribution of mitochondria to the induction of cell apoptosis is likely to be more important.

To evaluate the roles of caspases in 5FU-SeNP-induced apoptosis, several caspase inhibitors such as z-VAD-fmk (general caspase inhibitor), z-IETD-fmk (caspase-8 inhibitor), and z-LEHD-fmk (caspase-9 inhibitor), were used to be examined their effects on the cell apoptosis. As shown in Figure 9B, 5FU-SeNP-induced apoptotic cell death was remarkably suppressed by pretreatment with z-VAD-fmk, suggesting that 5FU-SeNP-induced apoptotic cell death occurs mainly in a caspase-dependent manner. Cell apoptosis was also suppressed by caspase-8 inhibitor from 34.5% to 23.2%, which confirms the contribution of death receptors to the cell apoptosis. Moreover, caspase-9 inhibitor more significantly decreased apoptotic cell death to 15.1%. These results further confirm the important role of the intrinsic mitochondrial-mediated apoptotic pathway in 5FU-SeNP-induced apoptosis.

5FU-SeNPs Induce Mitochondria-Mediated Apoptosis in a ROS-Dependent Manner. Mitochondria act as a point of integration for apoptotic signals originating from both the extrinsic and intrinsic apoptotic pathways.[41] Loss of $\Delta\Psi$m is associated with the activation of caspases and

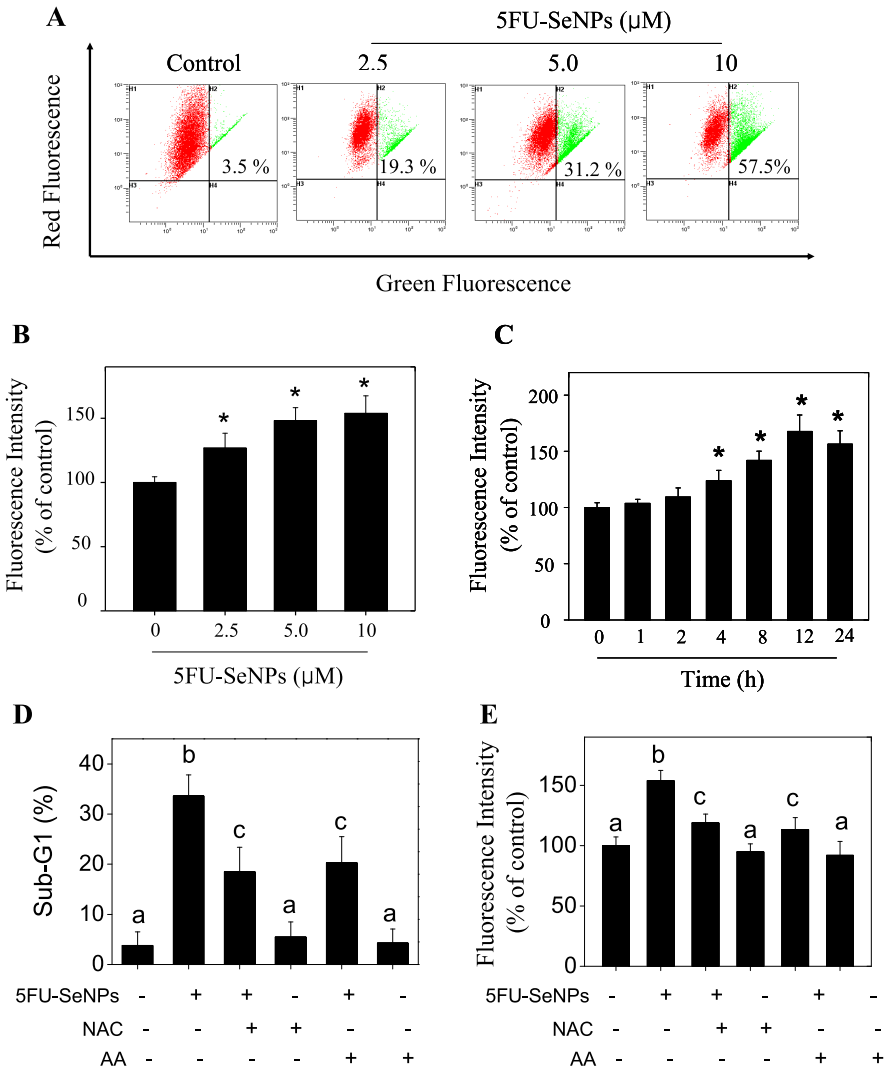

Figure 10. (A) Loss of mitochondrial membrane potential (ΔΨm) in A375 cells induced by 5FU-SeNPs. Cells treated with Se-PC were harvested and stained with JC-1 and then analyzed by flow cytometry. The number in the right region of each dot plot represents the percentage of cells that emit green fluorescence due to the loss of ΔΨm. 5FU-SeNP-induced apoptosis is dependent on ROS generation. (B) Cells were exposed to the indicated concentrations of 5FU-SeNPs for 3 h and the levels of the intracellular ROS were analyzed by DCFH-DA fluorescence intensity. (C) Cells were exposed to 40 μM 5FU-SeNPs for different times and the levels of the intracellular ROS were analyzed by DCFH-DA fluorescence intensity. (D, E) Effects of NAC and ascorbic acid (AA) on cell apoptosis and ROS generation induced by 5FU-SeNPs. Cells were pretreated with 2 mM NAC or 1 mM ascorbic acid (AA) for 4 h and then exposed to 10 μM 5FU-SeNPs for 24 h. Apoptotic cell death was determined by flow cytometric analysis. All results were obtained from three independent experiments. Significant difference between treatment and control groups is indicated at $P < 0.05$ (*) level. Bars with different characters (a, b, and c) are statistically different at the $P < 0.05$ level.

the initiation of apoptotic cascades. Thus, the status of mitochondria in A375 cells exposed to 5FU-SeNPs was examined by JC-1 flow cytometric analysis. As shown in Figure 10A, 5FU-SeNPs induced a dose-dependent increase in depletion of ΔΨm, as evidenced by the shift of fluorescence from red to green. For instance, 5FU-SeNPs at the concentrations of 5 and 10 μM increased ΔΨm of cells from 3.5% to 31.2% and 57.5%, respectively. These results further confirmed that 5FU-SeNPs induced apoptosis in A375 cells through mitochondria-mediated pathways.

The mitochondrial respiratory chain is a potential source of ROS, such as hydrogen peroxide and superoxide. The generation of intracellular ROS may be related to mitochondrial dysfunction and the induction of apoptosis.[42,43] ROS has been reported as an important regulator of mitochondrial function.[44] A number of apoptotic stimuli induce cytochrome *c* release and apoptosis *via* ROS overproduction.[45] Therefore we examined the intracellular ROS generation in A375 cells by measuring the DCF fluorescence intensity. This assay is based on the cellular uptake of a nonfluorescent probe (DCFH-DA), which is subsequently hydrolyzed by intracellular esterase to form dichlorofluorescin, DCFH. Figure 10B showed that 5FU-SeNP treatment dose-dependently increased DCF fluorescence intensity,

indicating the up-regulation of intracellular ROS levels. At the same time, Figure 10C showed the time course of ROS generation induced by the 5FU-SeNPs. The level of the intracellular ROS was significantly increased at 4 h after 5FU-SeNP treatment, which peaked at approximately 12 h, followed by a decreasing trend from 12 to 24 h. To further examine the important role of ROS generation in 5FU-SeNP-induced apoptosis, we next investigate the effects of a thiol-reducing antioxidant NAC and ascorbic acid (AA) on apoptotic cell death and intracellular ROS generation. The data revealed that NAC or AA effectively prevented the increase in sub-G1 cell populations (Figure 10D) and ROS overproduction (Figure 10E) induced by 5FU-SeNPs. These results suggest that 5FU-SeNP-induced apoptosis in A375 cells is ROS-dependent.

CONCLUSIONS

Our present works provide a design of drug delivery system by using SeNPs as a carrier of 5FU to achieve anticancer synergism. SeNPs were capped by 5FU through physical adsorption and the formation of Se−O and Se−N bonds. 5FU surface decoration significantly enhanced the cellular uptake of the SeNPs in cancer cells by endocytosis through clathrin- and caveolae-mediated pathways. 5FU molecules played an important role in the internalization process of the nanoparticles. The studies on *in vitro* drug release revealed that faster release of 5FU has been observed under the acidic condition, which is exactly what we expect. 5FU thus could principally be distributed around tumor tissues with an acidic microenvironment rather than in the normal section. Therefore, SeNPs hold a promise as a pH-mediated release delivery vehicle for potential cancer therapy.

Se is an essential trace element with a narrow margin between beneficial and toxic effects. As a promising chemopreventive agent, its use requires consumption over the long-term. Therefore, the toxicity of Se is always a crucial concern. Many studies have support that the chemical forms and doses are important factors that may greatly affect the biological activities and toxicity of Se. A panel of five human cancer cell lines was shown to be susceptible to the 5FU-SeNPs, with IC_{50} values ranging from 6.2 to 14.4 μM. Despite this potency, the 5FU-SeNPs possess great selectivity between cancer and normal cells. *In vivo* animal studies also demonstrated that the acute lethal dose and the acute liver injury induced by 5FU-SeNPs were significantly lower than those of selenomethionine, a predominant chemical form of Se in foodstuffs. Our results indicate that the 5FU-SeNPs could serve as a potential anticancer agent with enhanced anticancer activities and reduced risk of Se toxicity. For the action mechanisms of the nanomaterials, our studies revealed that 5FU-SeNPs induced caspase-dependent apoptosis in A375 human melanoma cells mainly through activation of an intrinsic apoptotic pathway. Furthermore, 5FU-SeNPs-induced apoptosis was also found dependent on ROS generation. On the basis of these results, 5FU-SeNPs could be developed as novel apoptosis inducers against cancer cells.

However, limitation also exists in the 5FU-SeNPs. Although formulating Se in the form of nanoparticles effectively decrease its toxicity, the dose which would be administered to achieve a chemotherapeutic efficacy may still exceed the toxic threshold of Se. Second, the selectivity between cancer and normal cells in human bodies could be a challenge for the 5FU-SeNPs. However, a cancer-targeting design could be a good strategy to dissolve these two problems. For instance, antibodies, ligands, or aptamers that target cancer cells could be conjugated to the surface of the 5FU-SeNPs, which could provide preferential accumulation of nanoparticles in the tumor-bearing organ, enhance the selective killing abilities against cancer cells, and at the same time, reduce the toxicity toward normal cells. This functionalization may effectively avoid, at least minimize the toxicity of SeNPs. Alternatively, topical treatment is also an effective way to cure melanoma. Our results have showed that the melanoma cells displayed the highest sensitivity of the 5FU-SeNPs. Therefore, the topical drug delivery of the 5FU-SeNPs could be a reasonable strategy for the treatment of melanoma, which could effectively avoid the *in vivo* degradation of the 5FU-SeNPs. Actually, 5-FU cream and solution have been used to treat skin cancers in clinical settings. Therefore, the development of the 5FU-SeNPs as a topical therapeutic agent could be an achievable design for treatment of melanoma. However, pharmaceutics studies are needed to realize this design. Taken together, our results suggest that the strategy to use the SeNPs as a carrier of 5FU could be a highly efficient way to realize synergistic treatment of cancers. Furthermore, 5FU-SeNPs may be candidates for further evaluation as a chemotherapeutic agent for human cancers, especially melanoma.

MATERIALS AND METHODS

Materials. All chemicals were of reagent grade and used without further purification. Selenium dioxide (Na_2SeO_3), *N*-acetylcysteine (NAC), 5-fluorouracil, ascorbic acid, thiazolyl blue tetrazolium bromide (MTT), propidium iodide (PI), 2′,7′-dichlorofluorescein diacetate (DCF-DA), 5,5′,6,6′-tetrachloro-1,1′,3,3′-tetraethylimidacarbocyanine iodide (JC-1), and bicinchoninic acid (BCA) kit for protein determination were purchased from Sigma. Terminal transferase dUTP nick end labeling (TUNEL) assay kit was obtained from Roche Applied Science (Basel, Switzerland). Caspase-3 substrate (Ac-DEVD-AMC) was purchased from Biomol (Germany). Caspase-9 substrate (Ac-LEHD-AFC) and caspase-8 substrate (Ac-IETD-AFC) were purchased from Calbiochem. RPMI 1640 medium, DMEM medium and fetal

bovine serum (FBS) were purchased from Gibco BRL (Gaithersburg, MD). Milli-Q water was used in all experimental processes.

Preparation of 5FU-SeNPs. Before the experiments, a stock solution of 5 mM Na_2SeO_3 was prepared by dissolving 8.7 mg of sodium selenite (Na_2SeO_3) powder in 10 mL of Milli-Q water. Ascorbic acid (Vc) solution (20 mM) was freshly prepared before the experiments. A 5 mL aliquot of Na_2SeO_3 stock solution was mixed with 5 mL of 32.5 mg/mL 5FU solution. Then 5 mL of Vc solution was dropwise added, and the mixture was reconstituted to a final volume of 25 mL with Milli-Q water. Then the mixed solution was stirred for 24 h at room temperature and the final concentration of Na_2SeO_3 was 1.0 mM. Excess 5FU and Na_2SeO_3 were removed by dialysis against Milli-Q water overnight. Se concentration was determined by ICP−AES analysis. To determine the *in vitro* cellular uptake of 5FU-SeNPs, the nanoparticles containing a fluorescent dye 6-coumarin, were prepared using a similar procedure except that 100 μg of the dye was added to the reaction system after the addition of 5FU. The incorporated dye acts as a probe for 5FU-SeNPs and offers a sensitive method to determine their intracellular uptake and localization.

Characterization of 5FU-SeNPs. The as-prepared products were characterized by using microscopic and spectroscopic methods. Briefly, TEM samples were prepared by dispersing the powder onto a holey carbon film on copper grids. The micrographs were obtained on Hitachi (H-7650) for TEM operated at an accelerating voltage at 80 kV. Fourier transform infrared spectroscopy (FT-IR) spectra of the samples were recorded on Equinox 55 IR spectrometer in the range 4000−400 cm^{-1} using the KBr-disk method. The zeta potential and size distribution of the nanoparticles was measured by PCS on a Nano-ZS instrument (Malvern Instruments Limited). SEM-EDX analysis was carried out on an EX-250 system (Horiba) and employed to examine the elemental composition of the 5FU-SeNP powder.

XPS Measurements. XPS measurement was carried out on an ESCALab 250 spectrometer with the monochromatic Al Kα X-ray radiation (energy 1486.6 eV, 500 μm spot-size). A low-energy electron gun was used for the static charge compensation. The pass energy and step size were set at 150 and 1.0 eV for the survey scans and 20 and 0.1 eV for the narrow scans, respectively.

***In Vitro* Drug Release of 5FU.** A 10 mg aliquot of the 5FU-SeNPs was suspended in 10 mL of DMEM cell culture medium without 10% serum with constant shaking at 37 °C in a hard glass tube. At a specific time following incubation, a specific amount of medium was taken out from the vial with pipet and the same volume of fresh medium was replaced. All samples were analyzed using an HPLC system (Agilent 1100) with a model UV-1000 UV detector, and the detection wavelength was set at 266 nm. The column used was μ-Bondapak C_{18} (4 × 300 mm, Grom, Germany). Mobile phase was acetate buffer solution (pH = 4.7), and flow rate was adjusted at 1.0 mL/min.

Cell Lines and Cell Culture. Several human cell lines used in this study, including A375 melanoma cells, MCF-7 breast adenocarcinoma cells, HepG2 hepatocellular carcinoma cells, Colo201 colon adenocarcinoma cells, PC-3 prostatic csarcinoma cells, Hs68 human normal fibroblast cells, HK-2 proximal tubular cells and MCF-10A human mammary epithelial cells were purchased from American Type Culture Collection (ATCC, Manassas, VA). All cell lines were maintained in either RPMI-1640 or DMEM media supplemented with penicillin (100 units/mL), fetal bovine serum (10%), and streptomycin (50 units/mL) at 37 °C in a humidified incubator with 5% CO_2 atmosphere. Cholera toxin was added to the culture medium of MCF-10A cells at 100 ng/mL.

Generation of Murine Bone Marrow Macrophage. Primary cultures of bone marrow-derived macrophages (BMM) were obtained from BALB/c mice (Guangzhou, China). Briefly, bone marrow cells were flushed from the femur and tibia of female 6−8 weeks old mice and cultured for 7 days at a density of 5 × 10^5 cells/mL in IMDM supplemented with 15% Fetal Clone II (Perbio-science, France), penicillin−streptomycin (1 μg/mL), and 10 ng/mL macrophage-colony stimulating factor (M-CSF, Tebu-bio, France).

***In vitro* Cellular Uptake of 5FU-SeNPs.** For quantitative analysis of cellular uptake, A375 cells were seeded into 96-well plates at 8000 cells/well (0.1 mL) and allowed to attach for 24 h. The medium in the well was replaced with different concentrations of 6-coumarin-loaded 5FU-SeNPs and incubated for various periods of time at 37 °C in CO_2 incubator. At the end of the incubation, the medium was removed from the wells and the cells were rinsed three times with cold PBS to remove the nanoparticles outside the cells. After that, 100 μL of 0.5% Triton X-100 in 0.2 M NaOH solution was added to lyse the cells. Microplate reader (SpectraMax M5, MD, USA) was used to measure the fluorescence intensity from coumarin-6 loaded nanoparticles inside the wells with excitation and emission wavelengths set at 485 and 525 nm, respectively. The cellular uptake efficiency was expressed as the percentage of the fluorescence of the testing wells over that of the positive control wells. The medium used in this study was DMEM completed medium with the presence of 10% fetal bovine serum. A standard curve for the nanoparticles was constructed by suspending different concentrations of nanoparticles and treating them in a similar way as cell sample preparation. The uptake of 6-coumarin nanoparticles by various cancer and normal cells was calculated from the standard curve and expressed as the amount of nanoparticles (μg) taken up per 10^6 cells.

The cellular uptake of 5FU-SeNPs was also monitored qualitatively by fluorescence microscopy. Briefly, treated cells cultured on cover glass in 6-well plates until 70% confluence were incubated with different concentrations of 6-coumarin-loaded 5FU-SeNPs for various periods of time. The cells were then washed three times by PBS and examined under a fluorescence microscope (Nikon Eclipse 230 80i).

Cellular Uptake Pathways of 5FU-SeNPs. A375 cells seeding density will be kept at 10^5 cells/well in 6-well plates (Costar, Corning, NY). After 24-h incubation in complete medium, the inhibitors of endocytosis will be added into serum-free DMEM medium and the cells will be incubated for 1 h, except for nystatin and methyl-β-cyclodextrine which will only be incubated for 30 min. The medium would then be replaced with complete medium containing 10% FBS, 40 μg/mL 5FU-SeNPs, and the same inhibitors for another 4 h. The control samples would be seeded into serum-free medium without inhibitors before the addition of the 5FU-SeNPs. The inhibitors for endocytosis used in this study were applied at the following final concentrations: chlorpromazine hydrochloride 10 μg/mL, sucrose 0.45 M, dynasore 80 μM, indomethacin 1 μM, methyl-β-cyclodextrine (M-β-CD) 10 mM, and nystatin 5 mg/mL. After treatment, all the samples would be collected and applied to ICP-AES analysis for determination of Se concentration. For analysis of energy-dependent pathways, the cells will be incubated in complete medium containing 5FU-SeNPs at 4 °C for 4 h. Alternatively, the cells were incubated in medium containing 10 mM NaN_3 and 50 mM 2-deoxy-D-glucose.

Real-Time Living Cell Imaging. Real-time observation of the cellular uptake and localization of 5FU-SeNPs was monitored by living cell imaging. Briefly, A375 cells cultured in 35 mm confocal dish with coverglass bottom were stained with 1 ug/mL DAPI for nucleuses for 20 min. After being washed with PBS twice, cells were cultured in fresh medium containing 6-coumarin-loaded 5FU-SeNPs on a thermo-cell culture FCS2 chamber of Carl Zeiss Cell Observer (Jena, Germany). Cell images were captured with a monochromatic CoolSNAP FX camera (Roper Scientific, USA) and analyzed by using AxioVision 4.2 software (Carl Zeiss).

MTT Assay. Cell viability was determined by measuring the ability of cells to transform MTT to a purple formazandye.[46] Cells were seeded in 96-well tissue culture plates at 2.5 × 10^3 cells/well for 24 h. The cells were then incubated with 5FU-SeNPs at different concentrations for different periods of time. After treatment, 20 μL/well of MTT solution (5 mg/mL phosphate buffered saline) was added to the well and incubated for another 5 h. To dissolve the formazan salt formed, the medium was aspirated and replaced with 150 μL/well DMSO. The cell growth condition was reflected by the color intensity of the formazan solution. Absorbance at 570 nm was taken on a 96-well microplate reader (MD VERSA max).

Flow Cytometric Analysis. The cell cycle distribution was monitored by flow cytometric analysis. Briefly, the cells treated with or without 5FU-SeNPs were harvested and washed with PBS. After being fixed with 70% ethanol at −20 °C overnight, the cells were stained with propidium iodide (PI). Labeled cells were washed twice with PBS and then subjected to flow cytometric analysis. Cell cycle distribution was analyzed using MultiCycle software (Phoenix Flow Systems). The scale of cells in G0/G1, S, and G2/M phases was described as a DNA histogram. The apoptotic cells, with hypodiploid DNA content, were estimated through quantifying the sub-G1 peak in the cell cycle pattern. For each experiment, 10 000 events per sample were recorded.

TUNEL-DAPI Costaining Assay. DNA fragmentation induced by 5FU-SeNPs was examined by using an *in situ* cell death detection kit following the manufacturer's protocol. In short, cells cultured in chamber slides were fixed with 3.7% formaldehyde and then permeabilized with 0.1% Triton X-100 in PBS. The cells were incubated with a TUNEL reaction mixture for 1 h. For nuclear staining, cells were incubated with 1 μg/mL of DAPI for 15 min at 37 °C. Stained cells were then washed with PBS and examined on a fluorescence microscope (Nikon Eclipse 80i).

Caspase Activity Assay. Harvested cell pellets were suspended in cell lysis buffer and incubated on ice for 1 h. After centrifugation at 11000*g* for 30 min, supernatants were collected and immediately measured for protein concentration by a BCA kit. For caspase activity assay, the cell lysates were placed in 96-well plates and then the specific caspase substrates (Ac-DEVD-AMC for caspase-3, Ac-IETD-AMC for caspase-8, and Ac-LEHD-AMC for caspase-9) were added. Plates were then incubated at 37 °C for 1 h, and caspase activity was determined by fluorescence intensity with the excitation and emission wavelengths set at 380 and 440 nm, respectively.

Evaluation of Mitochondrial Membrane Potential ($\Delta\Psi$m). Treated cells cultured in 6-well plates were trypsinized, washed with PBS, and incubated with 0.5 mL of PBS buffer containing 10 mg/mL of JC-1 at 37 °C for 10 min. After that, the cells were centrifuged to remove the supernatant at once, and cell pellets were suspended in PBS and then analyzed by flow cytometry. The lost $\Delta\Psi$m cells were represented by the percentage of the green fluorescence from JC-1 monomers.

Measurement of Intracellular Reactive Oxygen Species (ROS) Generation. The cells were harvested by centrifugation at 370 g (20 °C, 5 min), washed twice with PBS, and then suspended in PBS (1×10^6 cells/mL). The collected cells suspension was incubated with DCFH-DA at a final concentration of 10 μM at 37 °C for 30 min. The cells were then incubated with 5FU-SeNPs at 37 °C for different periods of time. The intracellular ROS level can be determined by the measurement of the fluorescence intensity on a Tecan SAFIRE multifunctional monochromator based microplate reader.

Statistical and Synergy Analysis. All experiments were carried out at least in triplicate and results were expressed as mean ± standard deviation. Statistical analysis was performed using SPSS statistical program version 13 (SPSS Inc., Chicago, IL). The difference between two groups was analyzed by two-tailed Student's *t*-test. Differences with $P < 0.05$(∗) or $P < 0.01$(∗∗) were considered statistically significant. The difference between three or more groups was analyzed by one-way ANOVA multiple comparisons. The synergistic effect between 5FU and the SeNPs was evaluated by the isobologram method.[39] Briefly, a straight line was formed by plotting the IC_{50} values of 5FU and SeNPs on the *x*- and *y*-axes, respectively. The data point in the isobologram corresponds to the actual IC_{50} value of 5FU-SeNPs. If a data point is on or near the line, this represents an additive treatment effect, whereas a data point that lies below or above the line indicates synergism or antagonism, respectively. Moreover, the combination index (CI) was also calculated to examine the interaction between 5FU and the SeNPs. A CI value of 1 indicates an additive effect between two drugs. Synergism is reflected by a combination index of <1, whereas antagonism is reflected by a combination index of >1.

Conflict of Interest: The authors declare no competing financial interest.

Acknowledgment. This work was supported by Natural Science Foundation of China and Guangdong Province, Program for New Century Excellent Talents in University, Key Project of Science and Technology, Department of Guangdong Province, the Fundamental Research Funds for the Central Universities and China Postdoctoral Science Foundation.

Supporting Information Available: Supplemental experimental procedures; XPS spectra of O 1s and N 1s in 5FU and 5FU-SeNPs; fluorescence spectra of 6-coumarin loaded 5FU-SeNPs and SeNPs; effects of 5FU on the cellular uptake efficiency of 5FU-SeNPs; *in vitro* release profiles of 5-FU from 5FU-SeNPs in PBS; growth inhibition of 5FU-SeNPs and 5FU and SeNPs against A375 cells; acute liver injury induced by 5FU-SeNPs and selenomethionine, and acute lethal effect of 5FU-SeNPs. This material is available free of charge *via* the Internet at http://pubs.acs.org.

REFERENCES AND NOTES

1. Ferlay, J.; Shin, H. R.; Bray, F.; Forman, D.; Mathers, C.; Parkin, D. M. Estimates of Worldwide Burden of Cancer in 2008: GLOBOCAN 2008. *Int. J. Cancer* **2010**, *127*, 2893–2917.
2. Yager, P.; Edwards, T.; Fu, E.; Helton, K.; Nelson, K.; Tam, M. R.; Weigl, B. H. Microfluidic Diagnostic Technologies for Global Public Health. *Nature* **2006**, *442*, 412–418.
3. Peer, D.; Karp, J. M.; Hong, S.; Farokhzad, O. C.; Margalit, R.; Langer, R. Nanocarriers as An Emerging Platform for Cancer Therapy. *Nat. Nanotechnol* **2007**, *2*, 751–760.
4. Farokhzad, O. C.; Langer, R. Impact of Nanotechnology on Drug Delivery. *ACS Nano* **2009**, *3*, 16–20.
5. Popova, N. V. Perinatal Selenium Exposure Decreases Spontaneous Liver Tumorogenesis in CBA Mice. *Cancer Lett.* **2002**, *179*, 39–42.
6. Redman, C.; Scott, J. A.; Baines, A. T.; Basye, J. L.; Clark, L. C.; Calley, C.; Roe, D.; Payne, C. M.; Nelson, M. A. Inhibitory Effect of Selenomethionine on the Growth of Three Selected Human Tumor Cell Lines. *Cancer Lett.* **1998**, *125*, 103–110.
7. Prokopczyk, B.; Rosa, J. G.; Desai, D.; Amin, S.; Sohn, O. S.; Fiala, E. S.; El-Bayoumy, K. Chemoprevention of Lung Tumorigenesis Induced by a Mixture of Benzo(a)pyrene and 4-(Methylnitrosamino)-1-(3-Pyridyl)-1-Butanone by the Organoselenium Compound 1,4-Phenylenebis(methylene)-selenocyanate. *Cancer Lett.* **2000**, *161*, 35–46.
8. Hu, H.; Li, G. X.; Wang, L.; Watts, J.; Combs, G. F., Jr.; Lu, J. Methylseleninic Acid Enhances Taxane Drug Efficacy against Human Prostate Cancer and Down-Regulates Antiapoptotic Proteins BCL-XL and Survivin. *Clin. Cancer Res.* **2008**, *14*, 1150–1158.
9. Li, S.; Zhou, Y.; Wang, R.; Zhang, H.; Dong, Y.; Ip, C. Selenium Sensitizes MCF-7 Breast Cancer Cells to Doxorubicin-Induced Apoptosis through Modulation of Phospho-AKT and its Downstream Substrates. *Mol. Cancer Ther.* **2007**, *6*, 1031–1038.
10. Yang, G. Q.; Xia, Y. M. Studies on Human Dietary Requirements and Safe Range of Dietary Intakes of Selenium in China and Their Application in the Prevention of Related Endemic Diseases. *Biomed. Environ. Sci.* **1995**, *8*, 187–201.
11. Reid, M. E.; Stratton, M. S.; Lillico, A. J.; Fakih, M.; Natarajan, R.; Clark, L. C.; Marshall, J. R. A Report of High-Dose Selenium Supplementation: Response and Toxicities. *J. Trace Elem. Med. Biol.* **2004**, *18*, 69–74.
12. Wang, H.; Zhang, J.; Yu, H. Elemental Selenium at Nano Size Possesses Lower Toxicity without Compromising the Fundamental Effect on Selenoenzymes: Comparison with Selenomethionine in Mice. *Free Radic. Biol. Med.* **2007**, *42*, 1524–1533.
13. Zhang, J.; Wang, X.; Xu, T. Elemental Selenium at Nano Size (Nano-Se) as a Potential Chemopreventive Agent with Reduced Risk of Selenium Toxicity: Comparison with Se-methylselenocysteine in Mice. *Toxicol. Sci.* **2008**, *101*, 22–31.
14. Park, K.; Lee, S.; Kang, E.; Kim, K.; Choi, K.; Kwon, I. C. New Generation of Multifunctional Nanoparticles for Cancer

Imaging and Therapy. *Adv. Funct. Mater.* **2009**, *19*, 1553–1566.
15. Cao, S.; Durrani, F. A.; Rustum, Y. M. Selective Modulation of the Therapeutic Efficacy of Anticancer Drugs by Selenium Containing Compounds against Human Tumor Xenografts. *Clin. Cancer Res.* **2004**, *10*, 2561–2569.
16. Card, J. W.; Magnuson, B. A. A Method to Assess the Quality of Studies That Examine the Toxicity of Engineered Nanomaterials. *Int. J. Toxicol.* **2010**, *29*, 402–410.
17. Zhang, J.; Wang, H.; Yan, X.; Zhang, L. Comparison of Short-Term Toxicity between Nano-Se and Selenite in Mice. *Life Sci.* **2005**, *76*, 1099–1109.
18. Takimoto, C. H.; Graham, M. A.; Lockwood, G.; Ng, C. M.; Goetz, A.; Greenslade, D.; Remick, S. C.; Sharma, S.; Mani, S.; Ramanathan, R. K.; Synold, T. W.; Doroshow, J. H.; Hamilton, A.; Mulkerin, D. L.; Ivy, P.; Egorin, M. J.; Grem, J. L. Oxaliplatin Pharmacokinetics and Pharmacodynamics in Adult Cancer Patients with Impaired Renal Function. *Clin. Cancer Res.* **2007**, *13*, 4832–4839.
19. Martenson, J. A.; Lipsitz, S. R.; Wagner, H., Jr; Kaplan, E. H.; Otteman, L. A.; Schuchter, L. M.; Mansour, E. G.; Talamonti, M. S.; Benson, A. B, 3rd Initial Results of a Phase II Trial of High Dose Radiation Therapy, 5-Fluorouracil, and Cisplatin for Patients with Anal Cancer (E4292): An Eastern Cooperative Oncology Group study. *Int. J. Radiat. Oncol. Biol. Phys.* **1996**, *35*, 745–749.
20. Saif, M. W.; Hashmi, S.; Mattison, L.; Donovan, W. B.; Diasio, R. B. Peripheral Neuropathy Exacerbation Associated with Topical 5-Fluorouracil. *Anticancer Drugs* **2006**, *17*, 1095–1098.
21. Boyer, J.; Maxwell, P. J.; Longley, D. B.; Johnston, P. G. 5-Fluorouracil: Identification of Novel Downstream Mediators of Tumour Response. *Anticancer Res.* **2004**, *24*, 417–423.
22. Kamoshida, S.; Shiogama, K.; Matsuoka, H.; Matsuyama, A.; Shimomura, R.; Inada, K.; Maruta, M.; Tsutsumi, Y. Immunohistochemical Demonstration of Dihydropyrimidine Dehydrogenase in Normal and Cancerous Tissues. *Acta Histochem. Cytochem.* **2003**, *36*, 471–479.
23. Visser, G. W.; Gorree, G. C.; Peters, G. J.; Herscheid, J. D. Tissue Distribution of [18F]-5-Fluorouracil in Mice: Effects of Route of Administration, Strain, Tumour and Dose. *Cancer Chemother. Pharmacol.* **1990**, *26*, 205–209.
24. Thant, A. A.; Wu, Y.; Lee, J.; Mishra, D. K.; Garcia, H.; Koeffler, H. P.; Vadgama, J. V. Role of Caspases in 5-FU and Selenium-Induced Growth Inhibition of Colorectal Cancer Cells. *Anticancer Res.* **2008**, *28*, 3579–3592.
25. Schroeder, C. P.; Goeldner, E. M.; Schulze-Forster, K.; Eickhoff, C. A.; Holtermann, P.; Heidecke, H. Effect of Selenite Combined with Chemotherapeutic Agents on the Proliferation of Human Carcinoma Cell Lines. *Biol. Trace Elem. Res.* **2004**, *99*, 17–25.
26. Fakih, M.; Cao, S.; Durrani, F. A.; Rustum, Y. M. Selenium Protects against Toxicity Induced by Anticancer Drugs and Augments Antitumor Activity: A Highly Selective, New, and Novel Approach for the Treatment of Solid Tumors. *Clin. Colorectal Cancer* **2005**, *5*, 132–135.
27. Kaur, G.; Iqbal, M.; Bakshi, M. S. Biomineralization of Fine Selenium Crystalline Rods and Amorphous Spheres. *J. Phys. Chem. C* **2009**, *113*, 13670–13676.
28. Li, Q.; Chen, T. F.; Yang, F.; Liu, J.; Zheng, W. J. Facile and Controllable One-Step Fabrication of Selenium Nanoparticles Assisted by L-Cysteine. *Mater. Lett.* **2010**, *64*, 614–617.
29. Villanueva, A.; de la Presa, P.; Alonso, J. M.; Rueda, T.; Martinez, A.; Crespo, P.; Morales, M. P.; Gonzalez-Fernandez, M. A.; Valdes, J.; Rivero, G. Hyperthermia HeLa Cell Treatment with Silica-Coated Manganese Oxide Nanoparticles. *J. Phy. Chem. C* **2010**, *114*, 1976–1981.
30. Acharya, S.; Dilnawaz, F.; Sahoo, S. K. Targeted Epidermal Growth Factor Receptor Nanoparticle Bioconjugates for Breast Cancer Therapy. *Biomaterials* **2009**, *30*, 5737–5750.
31. Chauhan, A.; Zubair, S.; Sherwani, A.; Owais, M. Aloe Vera Induced Biomimetic Assemblage of Nucleobase into Nanosized Particles. *PLoS One* **2012**, *7*, e32049.
32. Lozan, V.; Kersting, B. Synthesis, Characterisation and Crystal Structure of a Pd(II) Complex of a Heterocyclic Selenium(IV) Imide. *Dalton Trans.* **2007**, 4511–4513.
33. McAuley, B.; Cabaniss, S. E. Quantitative Detection of Aqueous Arsenic and Other Oxoanions Using Attenuated Total Reflectance Infrared Spectroscopy Utilizing Iron Oxide Coated Internal Reflection Elements to Enhance the Limits of Detection. *Anal. Chim. Acta* **2007**, *581*, 309–317.
34. Wohlhueter RM, M. R.; Plagemann, P. G. W. Facilitated Transport of Uracil and 5-Fluorouracil, and Permeation of Orotic Acid into Cultured Mammalian Cells. *J. Cell Physiol.* **1980**, *104*, 309–319.
35. Yamamoto, S.; Kawasaki, T. Active Transport of 5-Fluorouracil and Its Energy Coupling in Ehrlich Ascites Tumour Cells. *J. Biochem.* **1981**, *90*, 635–642.
36. Ojugo, A. S.; McSheehy, P. M.; Stubbs, M.; Alder, G.; Bashford, C. L.; Maxwell, R. J.; Leach, M. O.; Judson, I. R.; Griffiths, J. R. Influence of PH on the Uptake of 5-Fluorouracil into Isolated Tumour Cells. *Br. J. Cancer.* **1998**, *77*, 873–879.
37. Wang, F.; Wang, Y. C.; Dou, S.; Xiong, M. H.; Sun, T. M.; Wang, J. Doxorubicin-Tethered Responsive Gold Nanoparticles Facilitate Intracellular Drug Delivery for Overcoming Multidrug Resistance in Cancer Cells. *ACS Nano* **2011**, *5*, 3679–3692.
38. Imani, M.; Lahooti-Fard, F.; Taghizadeh, S. M.; Takrousta, M. Effect of Adhesive Layer Thickness and Drug Loading on Estradiol Crystallization in a Transdermal Drug Delivery System. *AAPS PharmSciTech* **2010**, *11*, 1268–1275.
39. Tallarida, R. J. Drug Synergism: Its Detection and Applications. *J. Pharmacol. Exp. Ther.* **2001**, *298*, 865–872.
40. Sinha, R.; El-Bayoumy, K. Apoptosis Is a Critical Cellular Event in Cancer Chemoprevention and Chemotherapy by Selenium Compounds. *Curr. Cancer Drug Targets* **2004**, *4*, 13–28.
41. Van Gurp, M.; Festjens, N.; van Loo, G.; Saelens, X.; Vandenabeele, P. Mitochondrial Intermembrane Proteins in Cell Death. *Biochem. Biophys. Res. Commun.* **2003**, *304*, 487–497.
42. Ghobrial, I. M.; Witzig, T. E.; Adjei, A. A. Targeting Apoptosis Pathways in Cancer Therapy. *CA Cancer J. Clin.* **2005**, *55*, 178–194.
43. Fulda, S.; Debatin, K. M. Extrinsic *versus* Intrinsic Apoptosis Pathways in Anticancer Chemotherapy. *Oncogene* **2006**, *25*, 4798–4811.
44. Dhanasekaran, A.; Kotamraju, S.; Karunakaran, C.; Kalivendi, S. V.; Thomas, S.; Joseph, J.; Kalyanaraman, B. Mitochondria Superoxide Dismutase Mimetic Inhibits Peroxide-Induced Oxidative Damage and Apoptosis: Role of Mitochondrial Superoxide. *Free Radic. Biol. Med.* **2005**, *39*, 567–583.
45. Apel, K.; Hirt, H. Reactive Oxygen Species: Metabolism, Oxidative Stress, and Signal Transduction. *Annu. Rev. Plant. Biol.* **2004**, *55*, 373–399.
46. Chen, T.; Wong, Y. S. Selenocystine Induces Reactive Oxygen Species-Mediated Apoptosis in Human Cancer Cells. *Biomed. Pharmacother.* **2009**, *63*, 105–113.